

Dynamical fluctuating charge force fields: Application to liquid water

Steven W. Rick, Steven J. Stuart, and B. J. Berne

Department of Chemistry and Center for Biomolecular Simulation, Columbia University, New York, New York 10027

(Received 2 May 1994; accepted 14 June 1994)

A new molecular dynamics model in which the point charges on atomic sites are allowed to fluctuate in response to the environment is developed and applied to water. The idea for treating charges as variables is based on the concept of electronegativity equalization according to which: (a) the electronegativity of an atomic site is dependent on the atom's type and charge and is perturbed by the electrostatic potential it experiences from its neighbors and (b) charge is transferred between atomic sites in such a way that electronegativities are equalized. The charges are treated as dynamical variables using an extended Lagrangian method in which the charges are given a fictitious mass, velocities, and kinetic energy and then propagated according to Newtonian mechanics along with the atomic degrees of freedom. Models for water with fluctuating charges are developed using the geometries of two common fixed-charge water potentials: the simple point charge (SPC) and the four-point transferable intermolecular potential (TIP4P). Both fluctuating charge models give accurate predictions for gas-phase and liquid state properties, including radial distribution functions, the dielectric constant, and the diffusion constant. The method does not introduce any new intermolecular interactions beyond those already present in the fixed charge models and increases the computer time by only a factor of 1.1, making this method tractable for large systems.

I. INTRODUCTION

In simple molecular force fields, the intramolecular electronic structure is often modeled by point charges fixed on well-defined sites in the molecular frame. The charges are constant and thus cannot change in response to changing electrostatic fields which arise from movement of the atoms during the simulation. In reality, molecular electronic structure can be strongly influenced by the molecular environment. For example, the total dipole moment of water changes from 1.85 D in the gas phase to approximately 2.5 D in the liquid phase. Thus the charges used in simulations based on fixed charge force fields must reflect average or mean field charge values for the particular phase and are not transferable to different thermodynamic states or to different media. In addition, the self-energy involved in the change in charge accompanying the transition from gas phase to liquid phase is commonly neglected in most force field parametrizations. This "missing term" in fixed charge pair potentials can be significant (2 to 5 kcal/mol for water).¹ Charge induction effects are not pairwise additive and improved models must go beyond pair potentials. The purpose of this paper is to present a new simulation method in which the charges are responsive to environmental changes.

The approach taken here combines the electronegativity equalization (EE) method for determining atomic charges and the extended Lagrangian method for treating fictitious degrees of freedom as dynamical variables. The calculation of atomic electronegativities using density functional theory, basis set methods, or empirical data and the use of this information to estimate charges for large molecules has a long history.²⁻⁷ The electronegativity of an atomic site is dependent on its charge and the electronegativities of the neighboring atoms. Parr has shown that the Mulliken electronegativity (χ_i) of an isolated atom i is the negative of the chemical

potential (μ_i) of the electron gas surrounding its nucleus

$$\mu_i = \frac{\partial E}{\partial N} = -\chi_i = -e \frac{\partial E}{\partial Q_i}, \quad (1.1)$$

where E is the ground state energy, N is the number of electrons in the atom (treated as a continuous variable), Q is the charge on the atom, and e is the elementary charge. Use has been made of the fact that Q is related to N by $Q = -e(N - Z)$, where Z is the atomic number of the atom. In a many-atom system, the electron gas will equilibrate with the instantaneous positions of the nuclei in such a way that the electrochemical potential of the electron gas will be equal at all atomic sites. In this picture, electrons will then move among atoms from regions of low electronegativity (or high electrochemical potential) to regions of high electronegativity (low electrochemical potential). For the ground state electronic configuration, the electrochemical potentials are equal. The approach we take is to treat charges on the molecular sites as dynamical variables by introducing fictitious kinetic energy terms and self-energy terms for these charges into the Lagrangian for the system along with Lagrange constraints representing various conditions of electroneutrality. In this extended Lagrangian approach,⁸⁻¹¹ the charges are propagated according to Newtonian mechanics in a similar way to the atomic degrees of freedom. Although the fluctuating charge model provides a convenient starting point for the discussion of complex solutes like n -methylacetamide and proteins, we focus here on its application to the simulation of neat water.

Liquid water was chosen for the first application of this fluctuating charge (or fluc- q) model because charge polarization effects should be important for water. Simple water models, such as the simple point charge (SPC)¹² or the four-point transferable intermolecular potential (TIP4P),¹³ with a

Lennard-Jones interaction between oxygen atoms and three charge sites with fixed liquid state charges, can give accurate predictions for many equilibrium properties of liquid water, including the energy and radial distribution functions. Due to their simplicity and relative accuracy, these are perhaps the two most widely used water potentials. However, the translational and rotational time scales of these models are too fast, although the SPC/E¹ reparametrization gives improved relaxation times. More importantly, these models are unable to deal accurately with heterogeneous environments. Simulations of sodium octanoate micelles in SPC water predict too much penetration of water molecules into the micelle^{14,15} in contrast to experiments.¹⁶ The purpose of this paper is to add fluctuating charges to the SPC and TIP4P potentials and to thus devise a model which has improved static and dynamical properties relative to the fixed charge models and which is easily extended to more complex solutions.

Electrical induction can also be described to lowest order using fixed gas phase charges and point polarizabilities. Many dipole polarization models have been used to simulate liquid water.^{17–25} The fluc-*q* model presented here is an alternative which differs from the dipole polarizable models in two respects. First, the fluc-*q* models have polarizabilities to all orders in the charge moments and not only dipolar polarizability. In addition, the dipole polarizability models introduce a new interaction (the $1/r^3$ dipole-dipole interaction) and in order to solve for the induced dipole moments, either the induced dipole equations are solved iteratively, by matrix inversion, or the polarizations are treated in an extended Lagrangian framework. The iterative solution method increases the cost by a factor of 2 (Ref. 23) and the extended Lagrangian methods by a factor of 2 (Ref. 26) to 4.²⁰ The fluc-*q* method introduces no new intermolecular interactions beyond the fixed-charge models and increases the CPU time by a factor of only 1.1. Of course the dipole polarizability model can also be cast in terms of Drude dispersion oscillators, a system that also lends itself to treatment by the extended Lagrangian method.

This paper is organized as follows: Section II describes the fluc-*q* method and the form of the water-water interactions. Section III describes our implementation of molecular dynamics. Section IV describes the results of these models and Sec. V summarizes the conclusions.

II. DYNAMICAL FLUCTUATING CHARGE MODELS

The central idea for treating charges as dynamical variables is based on the electronegativities of atomic sites. Parr has shown, using the Kohn-Sham theory, that in an atom, the atomic electrons, regarded as an electron gas, have a chemical potential which is the negative of the Mulliken electronegativity.² In a many-atom system, the full electron gas will distribute itself so that its electrochemical potential takes the same value at every nuclear site. This principle of electronegativity equalization (EE) was first proposed by Sanderson.²⁷ If a given site moves so that it feels a different electrostatic potential, it will take on a different charge. In this way, the charges on molecular sites will respond to the environment.

In the isolated atom, the energy of creating a partial charge Q_A can be expanded to second order as

$$E(Q_A) = E_A(0) + \tilde{\chi}_A^0 Q_A + \frac{1}{2} J_{AA}^0 Q_A^2, \quad (2.1)$$

where $\tilde{\chi}_A^0$ and J_{AA}^0 are parameters dependent on the atom type. Values of $\tilde{\chi}_A^0$ and J_{AA}^0 can be calculated using basis set, density functional theory methods or empirical data. $\tilde{\chi}_A^0$ is the Mulliken electronegativity (per electronic charge e) and J_{AA}^0 is twice the hardness of the electronegativity of the isolated atom. The energy of a system of N_{molec} molecules each with N_{atom} atoms is

$$U[(\mathbf{Q}), (\mathbf{r})] = \sum_{i=1}^{N_{\text{molec}}} \sum_{\alpha=1}^{N_{\text{atom}}} \left[E_{\alpha}(0) + \tilde{\chi}_{\alpha}^0 Q_{i\alpha} + \frac{1}{2} J_{\alpha\alpha}^0 Q_{i\alpha}^2 \right] \\ + \sum_{i\alpha < j\beta} J_{\alpha\beta}(r_{i\alpha j\beta}) Q_{i\alpha} Q_{j\beta} \\ + \sum_{i\alpha < j\beta} V(r_{i\alpha j\beta}), \quad (2.2)$$

where $E_{\alpha}(0)$ is the ground state energy of atom α , $r_{i\alpha j\beta}$ is the distance, $J_{\alpha\beta}(r_{i\alpha j\beta})$ is the Coulomb interaction, and $V(r_{i\alpha j\beta})$ is any additional non-Coulombic interaction between $i\alpha$ and $j\beta$. The electronegativity per unit charge of atom A is given by

$$\tilde{\chi}_A = \left(\frac{\partial U}{\partial Q_A} \right). \quad (2.3)$$

The charges, by the EE principle, are then those for which the electronegativities are equal. This is equivalent to minimizing the energy, subject to a charge neutrality constraint. Since the potential is quadratic in the charges, the minimization will lead to a set of coupled linear equations for the charge.

The charges are not independent variables since there is a charge conservation constraint. For uncharged molecular systems, the constraint can be of two types:

- (1) The entire system is constrained to be neutral, so individual molecules can carry a nonzero charge because there can be intermolecular charge transfer

$$\sum_{i=1}^{N_{\text{molec}}} \sum_{\alpha=1}^{N_{\text{atom}}} Q_{i\alpha} = 0. \quad (2.4a)$$

Each molecule is constrained to be neutral, so there is no intermolecular charge transfer. Thus for all i

$$\sum_{\alpha=1}^{N_{\text{atom}}} Q_{i\alpha} = 0. \quad (2.4b)$$

With intermolecular charge transfer, the chemical potentials of all the atoms of the system will be equal. Without charge transfer, the chemical potential of an atom will only be equal to the chemical potential of atoms on the same molecule. The simplest way to treat the charge neutrality constraint is to

treat the charges as independent and use the method of undetermined multipliers to enforce the constraint. The Lagrangians for cases (1) and (2) are

$$L_1 = \sum_{i=1}^{N_{\text{molec}}} \sum_{\alpha=1}^{N_{\text{atom}}} \frac{1}{2} m_{\alpha} \dot{r}_{i\alpha}^2 + \sum_{i=1}^{N_{\text{molec}}} \sum_{\alpha=1}^{N_{\text{atom}}} \frac{1}{2} M_Q \dot{Q}_{i\alpha}^2 - U[(\mathbf{Q}), (\mathbf{r})] - \lambda \sum_{i=1}^{N_{\text{molec}}} \sum_{\alpha=1}^{N_{\text{atom}}} Q_{i\alpha} \quad (2.5a)$$

and

$$L_2 = \sum_{i=1}^{N_{\text{molec}}} \sum_{\alpha=1}^{N_{\text{atom}}} \frac{1}{2} m_{\alpha} \dot{r}_{i\alpha}^2 + \sum_{i=1}^{N_{\text{molec}}} \sum_{\alpha=1}^{N_{\text{atom}}} \frac{1}{2} M_Q \dot{Q}_{i\alpha}^2 - U[(\mathbf{Q}), (\mathbf{r})] - \sum_{i=1}^{N_{\text{molec}}} \lambda_i \sum_{\alpha=1}^{N_{\text{atom}}} Q_{i\alpha}, \quad (2.5b)$$

where m_{α} is the mass of atom α and M_Q is a fictitious charge "mass," which has units of energy time²/charge² and the λ are Lagrange multipliers. The nuclear degrees of freedom evolve according to Newton's equation

$$m_{\alpha} \ddot{r}_{i\alpha} = - \frac{\partial U[(\mathbf{Q}), (\mathbf{r})]}{\partial r_{i\alpha}} \quad (2.6)$$

and the set of charges evolve in time according to

$$M_Q \ddot{Q}_{i\alpha} = - \frac{\partial U[(\mathbf{Q}), (\mathbf{r})]}{\partial Q_{i\alpha}} - \lambda_i = - \tilde{\chi}_{i\alpha} - \lambda_i, \quad (2.7)$$

where λ_i is the Lagrange multiplier for the charge neutrality constraint, given either by Eq. (2.4a) or Eq. (2.4b). It should be noted that if the total charge in the liquid is a constant of the motion, then

$$\sum_{i=1}^{N_{\text{molec}}} \sum_{\alpha=1}^{N_{\text{atom}}} \ddot{Q}_{i\alpha} = 0, \quad (2.8a)$$

whereas if the total charge on molecule i is a constant of the motion, then for all i

$$\sum_{\alpha=1}^{N_{\text{atom}}} \ddot{Q}_{i\alpha} = 0. \quad (2.8b)$$

Substitution of Eq. (2.7) into each of the above two equations yields, respectively,

$$\lambda = - \frac{1}{N_{\text{molec}} N_{\text{atom}}} \sum_{i=1}^{N_{\text{molec}}} \sum_{\alpha=1}^{N_{\text{atom}}} \tilde{\chi}_{i\alpha} \quad (2.9a)$$

where λ is equal to the negative of the average of the system's total electronegativity and

$$\lambda_i = - \frac{1}{N_{\text{atom}}} \sum_{\alpha=1}^{N_{\text{atom}}} \tilde{\chi}_{i\alpha}, \quad (2.9b)$$

where λ_i is the negative of the average electronegativity on molecule i . Substitution of Eqs. (2.9a) and (2.9b) into the equations of the motion for the charges gives

$$M_Q \ddot{Q}_{i\alpha} = - \frac{1}{N_{\text{molec}} N_{\text{atom}}} \sum_{i=1}^{N_{\text{molec}}} \sum_{\beta=1}^{N_{\text{atom}}} (\tilde{\chi}_{i\alpha} - \tilde{\chi}_{i\beta}) \quad (2.10a)$$

and

$$M_Q \ddot{Q}_{i\alpha} = - \frac{1}{N_{\text{atom}}} \sum_{\beta=1}^{N_{\text{atom}}} (\tilde{\chi}_{i\alpha} - \tilde{\chi}_{i\beta}). \quad (2.10b)$$

Whether or not charges are allowed to transfer between atoms of different molecules or just between atoms on the same molecule makes little difference in the algorithm. The force on the charge is simply the difference between the average electronegativity and the instantaneous electronegativity at that site. For example, if the electronegativity is greater than the average, then the force acts to decrease the charge until the electronegativities are all equal. In the present application, we have included a charge neutrality constraint on each water molecule; there is no charge transfer between molecules [case (2)].

There have been many different applications of the EE principle, with differing values for the parameters $\tilde{\chi}_A$ and J_{AA} (some with higher order terms) which have been applied to a variety of molecules.³⁻⁷ Some of these applications have been used as potential input into simulations. However, in order to fully treat the charge fluctuations which arise in the course of a simulation, each new configuration would require the calculation of a new set of charges. This can be done by simply using the extended Lagrangian method to derive the equations of motion for Hamiltonians which depend on auxiliary degrees of freedom.^{8,10}

The above approach in which there is intermolecular charge transfer makes no allowance for the possibility that there can be barriers to the charge transfer preventing charge equilibration. Thus, e.g., two atomic sites separated by a great distance will in reality not transfer charges because the probability of tunneling through a wide barrier is small, yet the above model will allow charge transfer. This poses a major problem in principle when molecules are separated *in vacuo*, a problem that also exists in the Car-Parrinello method.¹⁰ For this reason, we have restricted the charge equilibration to intramolecular charge transfer. It would be useful to generalize this model to include such kinetic restrictions on charge transfer.

The charge mass M_Q , a fictitious quantity, should be chosen to be small enough to guarantee that the charges readjust very rapidly to changes in the nuclear degrees of freedom. This is equivalent to the Born-Oppenheimer adiabatic separation between the electronic and nuclear degrees of freedom. When M_Q is sufficiently small, there will be essentially no thermal coupling between the nuclear and electronic degrees of freedom. For numerical convenience, we choose the mass small enough to satisfy the foregoing requirement, yet large enough so that the time step required for the solution of the equations of motion is not too small. The charge degrees of freedom are to remain near 0 K, since they are to be near the values which minimize the electrostatic energy. Within the context of molecular dynamics, this can be achieved by Nosé thermostatting¹¹ the charge at a much lower temperature (~ 5 K) than the nuclei as is done in Car-

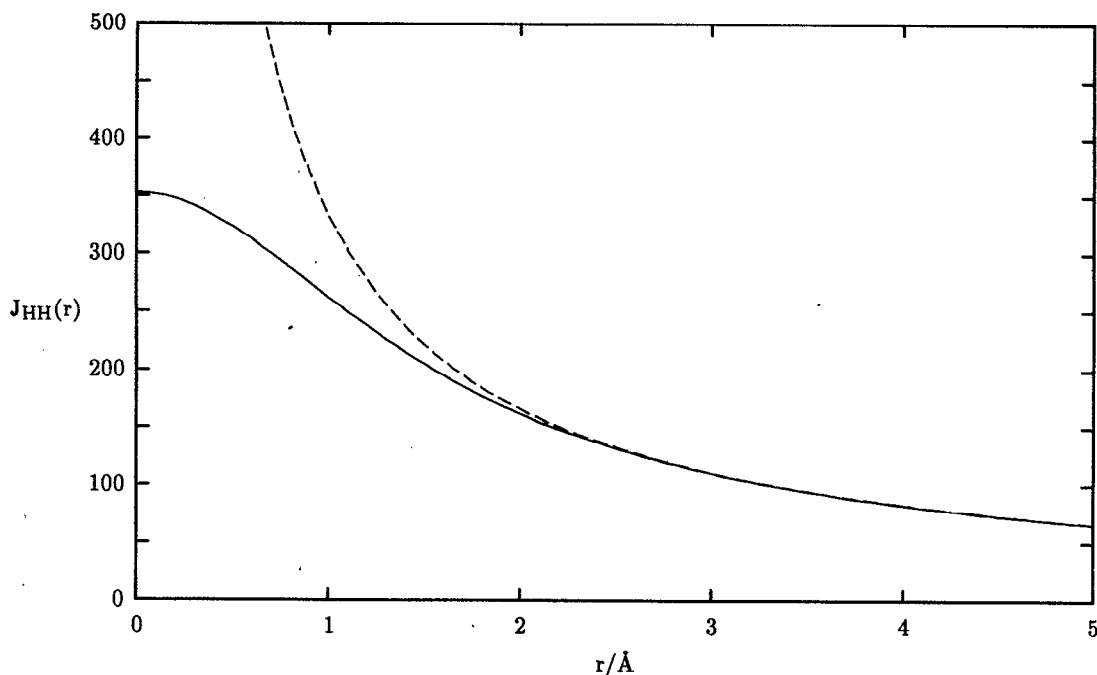


FIG. 1. Coulomb interaction for H-H pairs, comparing the intramolecular Coulomb overlap interaction (solid line) with the intermolecular pure Coulomb $1/r$ interaction (dotted line), in kcal/mol/ e^2 .

Parrinello *ab initio* molecular dynamics.²⁸⁻³⁰ However, with a charge mass of 6.0×10^{-5} for the TIP4P-FQ model and 6.9×10^{-5} (ps/e)² kcal/mol for the SPC-FQ model and a 1 fs time step for both models, there is almost no thermal coupling and the charge degrees of freedom remain at a temperature of less than 6 K for the duration of a 50 ps simulation. For simulations of this duration or shorter, no thermostatting is needed to keep the charge degrees of freedom near 0 K and the atomic degrees of freedom near the desired, much higher temperature. With this time step and M_Q , the fluc- q models have the same energy conservation as the fixed charge models. However, that small charge mass requires the use of a time step no greater than about 1 fs. This problem could be surmounted using multiple time scale molecular dynamics.³¹

Following Rappé and Goddard,⁶ the Coulomb interaction $J_{ij}(r)$ for intramolecular pairs is taken to be the Coulomb overlap integral between Slater orbitals centered on each atomic site

$$J_{ij}(r) = \int d\mathbf{r}_i d\mathbf{r}_j |\phi_{n_i}(r_i)|^2 \frac{1}{|\mathbf{r}_i - \mathbf{r}_j - \mathbf{r}|} |\phi_{n_j}(r_j)|^2. \quad (2.11)$$

The Slater orbitals are given by

$$\phi_{n_i}(r) = A_i r^{n_i-1} e^{-\zeta_i r} \quad (2.12)$$

and are characterized by a principal quantum number n_i and an exponent ζ_i . A_i is a normalization factor. The value of $J_{ii}(r)$ for $r=0$ is J_{ii}^0 and therefore the value of ζ_i uniquely determines J_{ii}^0 . For hydrogen, $n_H=1$ and $J_{HH}^0 = \frac{5}{8}\zeta_H$, and for oxygen, $n_O=2$ and $J_{OO}^0 = (93/256)\zeta_O$. The intermolecular

Coulomb interaction is set equal to the pure Coulomb interaction $1/r$ for consistency with other force fields. The interaction J_{HH} is shown in Fig. 1.

Two different water geometries were used, corresponding to the commonly used SPC¹² and TIP4P¹³ water models. Both of these models have three charged sites, two positive charged hydrogen sites, and a negative charged site, and a Lennard-Jones interaction between oxygen sites

$$U_{LJ}(r) = 4 \epsilon \left[\left(\frac{\sigma}{r} \right)^{12} - \left(\frac{\sigma}{r} \right)^6 \right] \quad (2.13)$$

TABLE I. Potential parameters for the fixed-charge potentials SPC and TIP4P and the flexible charge SPC and TIP4P (SPC-FQ, TIP4P-FQ) models. The last four terms J_{AB} are determined by ζ_H and ζ_O and so are not independent parameters.

	SPC ^a	TIP4P ^b	SPC-FQ	TIP4P-FQ
ϵ (kcal/mol)	0.1554	0.1550	0.2941	0.2862
σ (Å)	3.166	3.154	3.176	3.159
θ_{HOH} (degrees)	109.47	104.52	109.47	104.52
r_{OH} (Å)	1.0	0.9572	1.0	0.9572
r_{OM} (Å)	0.0	0.15	0.0	0.15
Q_H (e)	0.41	0.52		
$\bar{\chi}_O - \bar{\chi}_H$ [kcal/(mol e)]			73.33	68.49
ζ_O (a_0^{-1})			1.61	1.63
ζ_H (a_0^{-1})			1.00	0.90
J_{OO}^0 [kcal/(mol e^2)]			367.0	371.6
J_{HH}^0 [kcal/(mol e^2)]			392.2	353.0
$J_{\text{OH}}(r_{\text{OH}})$ [kcal/(mol e^2)]			276.0	286.4
$J_{\text{HH}}(r_{\text{HH}})$ [kcal/(mol e^2)]			196.0	203.6

^aReference 12.

^bReference 13.

with a well depth ϵ and a diameter σ . The SPC potential places the negatively charged site on the oxygen position; the TIP4P potential places this site (called the "M site") a distance of 0.15 Å from the oxygen position along the dipole direction toward the center of mass. The O–H bond length and H–O–H bond angle for the potentials are listed on Table I. The TIP4P model has the added complexity (and computational cost) of an additional interaction site, but has the correct water geometry. The potential energy contains the Lennard-Jones part [Eq. (2.13)] and the electrostatic part [Eq. (2.2)], and since we are defining the energies relative to the isolated gas-phase energy, the gas phase energy E_{gp} needs to be subtracted. For the isolated gas phase water molecule, the charge constraint gives $Q_O = -2Q_H$ and it is straightforward to find that the charge which minimizes the energy is

$$Q_H^{gp} = \frac{(\tilde{\chi}_O^0 - \tilde{\chi}_H^0)}{2J_{OO}^0 + J_{HH}^0 - 4J_{OH}(r_{MH}) + J_{HH}(r_{HH})} \quad (2.14)$$

and the gas phase energy is thus

$$E_{gp} = \frac{-(\tilde{\chi}_O^0 - \tilde{\chi}_H^0)^2}{2J_{OO}^0 + J_{HH}^0 - 4J_{OH}(r_{MH}) + J_{HH}(r_{HH})}, \quad (2.15)$$

where r_{MH} is the distance between the hydrogen and the M site for the TIP4P model, and for the SPC model, it is the distance between the hydrogen and the oxygen site. We have dropped the charge independent term $[E_i(0)]$, taking this as our definition of the zero of energy. The total energy for N_{molec} molecules is a sum of the Lennard-Jones part, the intermolecular Coulomb part, an intramolecular self-energy, and the gas-phase energy correction, to give

$$E = \sum_{i=1}^{N_{molec}} \sum_{j<i} \left\{ 4\epsilon \left[\left(\frac{\sigma}{r_{iO,jO}} \right)^{12} - \left(\frac{\sigma}{r_{iO,jO}} \right)^6 \right] + \sum_{\alpha=1}^3 \sum_{\beta=1}^3 Q_{i\alpha} Q_{j\beta} / r_{i\alpha,j\beta} \right\} + \sum_{i=1}^{N_{molec}} \sum_{\alpha=1}^3 \left[\tilde{\chi}_\alpha^0 Q_{i\alpha} + \frac{1}{2} \sum_{\beta=1}^3 Q_{i\alpha} Q_{i\beta} J_{\alpha\beta}(r_{i\alpha,i\beta}) \right] - N_{molec} E_{gp}, \quad (2.16)$$

where $r_{i\alpha,j\beta}$ is $|r_{i\alpha} - r_{j\beta}|$ and $\alpha=O$ indicates the oxygen atom.³² For periodic systems using the Ewald sum, the energy is

$$E = \sum_{i=1}^{N_{molec}} \sum_{j<i} \left\{ 4\epsilon \left[\left(\frac{\sigma}{r_{iO,jO}} \right)^{12} - \left(\frac{\sigma}{r_{iO,jO}} \right)^6 \right] + \sum_{\alpha=1}^3 \sum_{\beta=1}^3 Q_{i\alpha} Q_{j\beta} \operatorname{erfc}(\kappa r_{i\alpha,j\beta}) / r_{i\alpha,j\beta} \right\} + \frac{1}{2} \frac{4\pi}{L^3} \sum_{\mathbf{G} \neq 0} \frac{1}{G^2} e^{-G^2/4\kappa^2} \times \left| \sum_i \sum_\alpha Q_{i\alpha} e^{i\mathbf{G} \cdot \mathbf{r}_{i\alpha}} \right|^2 + \sum_{i=1}^{N_{molec}} \sum_{\alpha=1}^3 \left\{ \tilde{\chi}_\alpha^0 Q_{i\alpha} + \frac{1}{2} \sum_{\beta=1}^3 Q_{i\alpha} Q_{i\beta} [J_{\alpha\beta}(r_{i\alpha,i\beta}) - \operatorname{erf}(\kappa r_{i\alpha,i\beta}) / r_{i\alpha,i\beta}] \right\} - N_{molec} E_{gp}, \quad (2.17)$$

where κ is a screening parameter, \mathbf{G} is a reciprocal lattice vector of the periodic simulation cells, $\operatorname{erf}(x)$ is the error function, $\operatorname{erfc}(x)$ is the complementary error function, and L is the side length of the primary simulation box.³³

There are three independent electrostatic parameters $\tilde{\chi}_O^0 - \tilde{\chi}_H^0$, ζ_O , and ζ_H since the energy is dependent on the difference of the atomic electronegativities and the Slater exponents describe $J(r)$. We have adjusted these three parameters plus the two Lennard-Jones parameters to obtain the correct gas-phase dipole moments and to optimize the energy, pressure, and pair correlation functions of the liquid. The parameters are given in Table I. In order to implement the fluc- q procedure for the rigid bond length and rigid angle potentials used here, the Coulomb overlap integral needs to be evaluated only at $r=0$ and at the intramolecular bond lengths r_{OH} and r_{HH} . These values are also given on Table I. This optimization procedure does not uniquely define a set of parameters and those listed in Table I are one possible good choice which leads to improved water properties relative to the fixed charge models, as discussed in the next section. The electrostatic parameters $\tilde{\chi}_O^0 - \tilde{\chi}_H^0$, J_{HH}^0 , and J_{OO}^0 are within the range of values used in previous EE models.³⁻⁷

III. NUMERICAL METHOD

The molecular dynamics simulations were performed on the Connection Machine CM-5 with 256 molecules. Periodic boundary conditions were imposed, using the Ewald sum for the long-ranged electrostatic potentials. The screening parameter κ was set to $5/L$ and 256 reciprocal lattice vectors were used in the Fourier space sum. A time step of 1 fs and the SHAKE algorithm for enforcing bond constraints were used.³³ The data reported in the next section is from 20 separate 50 ps runs for each FQ model. MD is implemented on the parallel architecture of the CM-5 by arranging data on a two-dimensional grid, so that each virtual node (i,j) contains all the information (namely, $r_{i\alpha,j\beta}$ and $\mathbf{Q}_{i\alpha} \cdot \mathbf{Q}_{j\beta}$) for the interactions between molecules i and j .³⁴ This is done as follows:

- (1) For $\alpha=1$ to $\alpha=N_{atoms}$, $\mathbf{r}_{i\alpha}$ is placed on the first row of an $N_{molec} \times N_{molec}$ array $[\mathbf{A}_\alpha(i,1) = \mathbf{r}_{i\alpha}]$ and the data are then spread through each row of the array using the parallel copy operation (this step takes 3% of one time step).

TABLE II. Properties for potentials with the TIP4P geometry: the fixed-charge TIP4P and Watanabe-Klein (WK) models; the SRWK dipole polarizable model (SRWK-P); and the flexible charge model (TIP4P-FQ). Properties listed are the the gas-phase dipole moment, the dipole polarizabilities α_{ii} (the y and z directions lie in the plane of the molecule, with the z axis along the C_2 axis), the energy of the dimer in its minimum energy configuration, the distance between oxygen atoms for the minimum dimer configuration, and properties of the liquid as indicated.

	TIP4P ^a	WK ^b	SRWK-P ^c	TIP4P-FQ	Experimental
Gas-phase dipole moment (Debye)	2.18	2.60	1.85	1.85	1.85 ^d
α_{zz} (Å ³)	0	0	1.44	0.82	1.468±0.003 ^e
α_{yy} (Å ³)	0	0	1.44	2.55	1.528±0.013 ^e
α_{xx} (Å ³)	0	0	1.44	0	1.415±0.013 ^e
Dimer energy (kcal/mol)	-6.3			-4.5	-5.4±0.7 ^f
Dimer O-O length (Å)	2.75			2.92	2.98 ^f
Liquid state properties ($T=298$ K, $\rho=1.0$ g/cm ³)					
Energy (kcal/mol)	-10.1 ^a	-10.2 ^b	-11.1 ^c	-9.9	-9.9 ^a
Pressure (kbar)	0.0 ^b	0.1 ^b	0.6 ^c	-0.16±0.03	0.0
Dipole moment (Debye)	2.18	2.60 ^b	2.63 ^c	2.62	
ϵ_0	53±2 ^g	80±8 ^b	86±10 ^c	79±8	78 ^b
ϵ_∞	1	1		1.592±0.003	1.79 ^h
Diffusion constant (10 ⁻⁹ m ² /s)	3.6±0.2 ^b	1.1±0.3 ^b	2.4±0.3 ^c	1.9±0.1	2.30 ⁱ
τ_{NMR} (ps)	1.4±0.2 ^b	3.8±0.3 ^b		2.1±0.1	2.1 ^j
τ_D (ps)	7±2 ^b	22±4 ^b		8±2	8.27±0.02 ^k

^aReference 13.

^bReference 36.

^cReference 37.

^dReference 55.

^eReference 38.

^fReference 56.

^gReference 51.

^hReference 46.

ⁱReference 57.

^jReference 54.

^kReference 47.

- (2) Similarly, $r_{i\alpha}$ is placed on the first column of a different matrix [$\mathbf{B}_\alpha(1,i)=r_{i\alpha}$] and spread through each column (3%).
- (3) Nearest image $r_{i\alpha,j\beta}$ values can now be computed from $\mathbf{A}_\alpha(i,j)$ and $\mathbf{B}_\beta(i,j)$ without any communication between different virtual nodes (14%).
- (4) A similar "spread-spread" algorithm is used to place $\mathbf{Q}_{i\alpha}$ and $\mathbf{Q}_{j\beta}$ on each virtual node i, j (3%) and $\mathbf{Q}_{i\alpha} \cdot \mathbf{Q}_{j\beta}$ is calculated (1%).
- (5) All pairwise forces and potential energy terms can be calculated on each virtual node without communication (the Lennard-Jones term takes about 3%, the real space Ewald term takes 33%, and the Coulomb self-term takes 3% of a time step). The Fourier part of the Ewald sum [see Eq. (2.17)] does not involve pair terms and is calculated separately from the N_{molec}^2 process (21%).
- (6) The total energy and the force on atom i from all other atoms j are found from a parallel add operation across the virtual nodes (10%).
- (7) The positions and charges are propagated using Eqs. (2.6) and (2.7) (0%), bond constraints are enforced using SHAKE (4%), and the steps are repeated.

On a 16 processor CM-5, we found performances of about 0.4 s/time step, which is about a factor of 10 faster than a comparable program on an IBM 580.³⁵ The CPU required for the fluctuating charge model is only a factor of 1.10 larger than for the corresponding fixed-charge model.

IV. RESULTS

The properties of the fixed-charge and fluc- q models for the water monomer, water dimer, and liquid water are listed in Tables II and III. Our reported error bars represent two standard deviation error estimates. Table II lists the results

for the TIP4P-FQ model, in comparison to other TIP4P geometry models TIP4P,¹³ the Watanabe-Klein (WK) model,³⁶ and the dipole polarizable SRWK (SRWK-P) model.³⁷ The SRWK model has a slightly different geometry than TIP4P, and the length r_{OM} is 0.26 Å rather than 0.15 Å. Table III lists the results for some of the many models with a SPC geometry, including SPC,¹² SPC/E,¹ polarizable SPC (PSPC),²¹ and flexible charge SPC (SPC-FQ). The TIP4P, WK, SPC, and SPC/E models are all nonpolarizable fixed-charge models, and the WK and SPC/E models include a correction for the polarization energy discussed below. The WK model also includes a correction for the quantum librational energy.

For the monomer, the electrostatic parameters are chosen to give the correct gas phase dipole moment. Another property of the isolated molecule is the dipole polarizability tensor α defined by

$$\boldsymbol{\mu}^{\text{ind}} = \alpha \cdot \mathbf{E}, \quad (4.1)$$

where $\boldsymbol{\mu}^{\text{ind}}$ is the dipole moment induced by the external electric field \mathbf{E} . $\boldsymbol{\mu}^{\text{ind}}$ can be determined by adding a term $-\boldsymbol{\mu} \cdot \mathbf{E}$ to Eq. (2.2) for the monomer and minimizing the total potential energy with respect to the charge. If the plane of the molecule is in the zy plane and the dipole (C_2 axis) is along the z direction, then it is found that

$$\alpha_{zz} = \frac{2z_{\text{MH}}^2}{2J_{\text{OO}}^0 + J_{\text{HH}}^0 - 4J_{\text{OH}}(r_{\text{MH}}) + J_{\text{HH}}(r_{\text{HH}})}, \quad (4.2)$$

$$\alpha_{yy} = \frac{r_{\text{HH}}^2/2}{J_{\text{HH}}^0 - J_{\text{HH}}(r_{\text{HH}})}, \quad \alpha_{xx} = 0,$$

where z_{MH} is the z component of the distance from the negative charge site (the M site for TIP4P, the oxygen site for

TABLE III. Properties for potentials with the SPC geometry: the fixed-charge SPC and SPC/E models; dipole polarizable model (PSPC); and the flexible charge model (SPC-FQ). Properties listed are the gas-phase dipole moment, the dipole polarizabilities α_{ii} (the y and z directions lie in the plane of the molecule, with the z-axis along the C_2 axis), the energy of the dimer in its minimum energy configuration, the distance between oxygen atoms for the minimum dimer configuration, and properties of the liquid as indicated.

	SPC ^a	SPC/E ^b	PSPC ^c	SPC-FQ	Experimental
Gas-phase dipole moment (Debye)	2.27	2.35	1.85	1.85	1.85 ^d
α_{zz} (\AA^3)	0	0	1.44	1.02	1.468 \pm 0.003 ^e
α_{yy} (\AA^3)	0	0	1.44	2.26	1.528 \pm 0.013 ^e
α_{xx} (\AA^3)	0	0	1.44	0	1.415 \pm 0.013 ^e
Dimer energy (kcal/mol)	-6.7			-4.4	-5.4 \pm 0.7 ^f
Dimer O-O length (\AA)	2.75			2.94	2.98 ^f
Liquid state properties ($T=298$ K, $\rho=1.0$ g/cm ³)					
Energy (kcal/mol)	-10.0 ^g	-9.9 ^h	-9.1 ^c	-9.9	-9.9 ⁱ
Pressure (kbar)	0.3 ^g	-0.08 \pm 0.04 ^h		0.03 \pm 0.05	0.0
Dipole moment (Debye)	2.27	2.35	2.9 ^c	2.83	
ϵ_0	68 \pm 7 ^j	67 \pm 10 ^h		116 \pm 18	78 ^k
ϵ_∞	1	1		1.606 \pm 0.002	1.79 ^k
Diffusion constant (10^{-9} m ² /s)	3.3 \pm 0.2 ^g	2.4 \pm 0.4 ^h	2.0 \pm 0.2 ^h	1.7 \pm 0.1	2.30 ^l
τ_{NMR} (ps)	1.1 \pm 0.2 ^g	1.9 \pm 0.1 ^h		2.2 \pm 0.1	2.1 ^m
τ_D (ps)	11 \pm 2 ^g	10 \pm 3 ^h		9 \pm 3	8.27 \pm 0.02 ⁿ

^aReference 12.

^bReference 1.

^cReference 21.

^dReference 55.

^eReference 38.

^fReference 56.

^gReference 36.

^hReference 44.

ⁱReference 13.

^jReference 58.

^kReference 46.

^lReference 57.

^mReference 54.

ⁿReference 47.

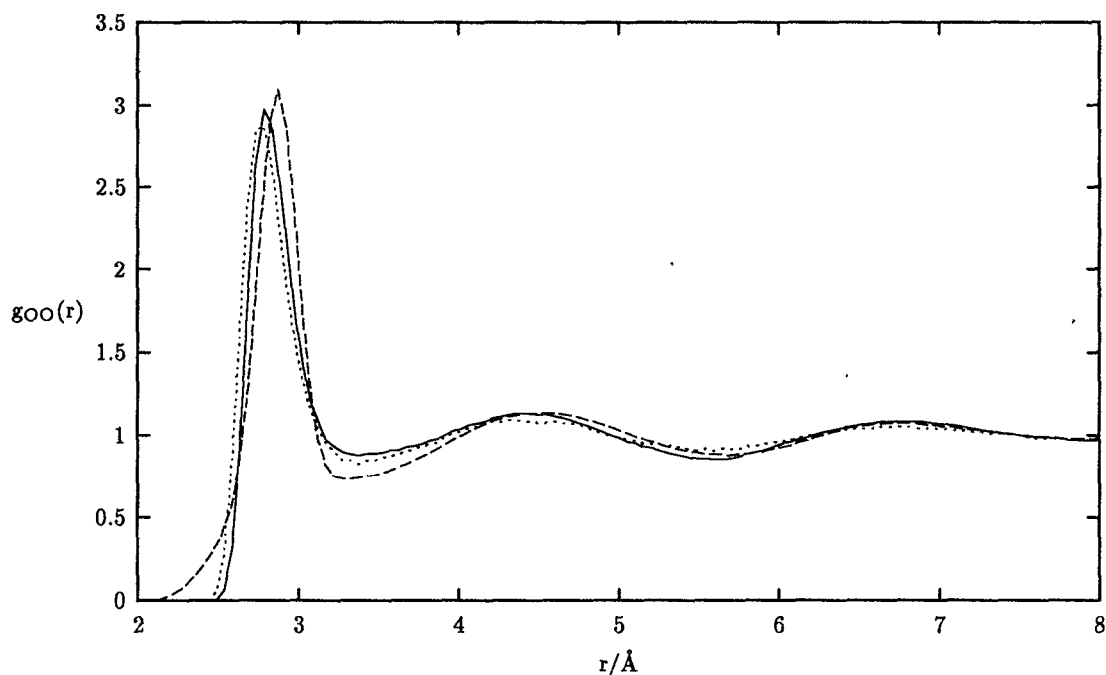


FIG. 2. Oxygen-oxygen radial distribution function for the TIP4P-FQ (solid line) and TIP4P (dotted line) potentials, compared to the neutron diffraction results of Soper and Phillips (dashed line).

SPC) to the positive charge sites, and α_{xx} is zero since all the charges are in the zy plane and no dipole induction is possible out of plane. Experimentally, α is almost isotropic,³⁸ so the lack of polarizability in the x direction is clearly a deficiency in fluc- q models, but corrections are possible.³⁹

The dimer properties listed in Tables II and III are the energy of the minimum energy configuration and the oxygen–oxygen distance of this configuration. Pair potentials, such as SPC and TIP4P, are parametrized to give the measured liquid state energies and radial distribution functions. It is known that this parametrization of these pairwise interaction models overestimates the gas phase water dimer energy. The fluctuating charge potentials predict an oxygen–oxygen separation closer to the experimental value, but underestimate the dimer energy.

We have calculated both static and dynamical properties of liquid state water at a temperature $T=298$ K and $\rho=1$ g/cm³. The error bars represent two standard deviations. The parameters for both fluc- q models are chosen to give a binding energy of -9.9 kcal/mol. This energy, unlike the fixed-charge potential energies, includes the self-polarization contribution arising from the difference in the internal energy given by Eq. (2.1) for the liquid state charges and the gas phase charges

$$\Delta E_{\text{self pol}} = \sum_{\alpha=1}^3 [\langle E_{\alpha}(Q_{\alpha}^{\text{liq}}) \rangle - E_{\alpha}(Q_{\alpha}^{\text{gas}})].$$

This self-polarization energy is the difference between the self-energy in the liquid phase and the gas phase Coulombic energy. The average self-polarization energy is 5.7 kcal/mol

for TIP4P-FQ and 7.6 kcal/mol for SPC-FQ, which represents a large contribution to the total energy. The dipole polarizable model of Sprik and Klein has a polarization energy of 5.9 kcal/mol. It has been noted that because the polarization energy is ignored in the parametrization of the SPC and TIP4P interaction potentials, these models underestimate the attractive pair interactions in water.¹ One simple correction for this is to subtract an estimate of the polarization energy $(\mu_{\text{liq}} - \mu_{\text{gas}})^2 / 2\alpha$ from the experimentally measured binding energy and to use the result to parametrize the pair potential. Here μ_{liq} and μ_{gas} are, respectively, the liquid state and gas phase permanent dipole moments used in the models. From this, it follows that the strength of the pairwise interaction must be increased to give the correct energy of -10 kcal/mol. This has been done for the SPC model (giving the SPC/E model¹) and TIP4P (giving the WK model³⁶), both of which have increased atomic charges and reduced diffusion constants compared to SPC or TIP4P.

The pair correlation functions give detailed information about the structure of the liquid. The TIP4P and TIP4P-FQ oxygen–oxygen radial distribution functions, $g_{\text{OO}}(r)$ are shown in Fig. 2 and are compared to the neutron diffraction results of Soper and Phillips.⁴⁰ Recent experiments of Soper and Turner indicate that there is a large experimental uncertainty in the peak heights of the pair correlation functions, perhaps due to the use of different methods for removing the contribution from self- or single atom scattering.⁴¹ The peak positions show much less uncertainty and therefore provide more reliable points for comparison. $g_{\text{OO}}(r)$ of the flexible charge model has a first peak at a larger r than the fixed

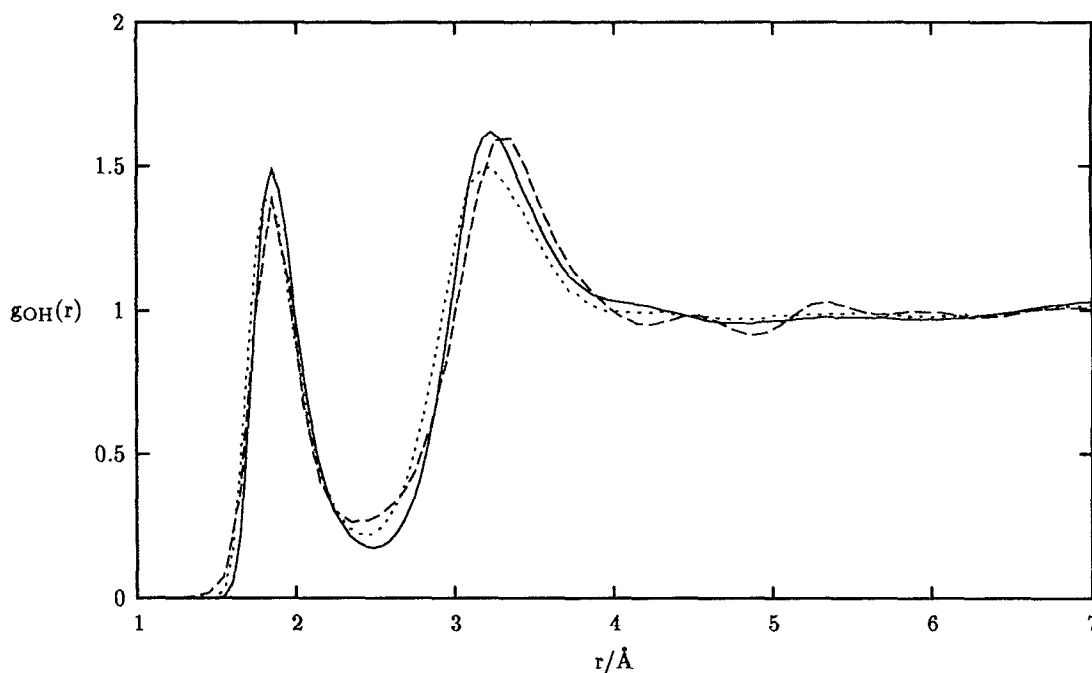


FIG. 3. Oxygen–hydrogen radial distribution function for the TIP4P-FQ (solid line) and TIP4P (dotted line) potentials, compared to the neutron diffraction results of Soper and Phillips (dashed line).

charge model and shows more long-ranged ordering due to the increased charges. The oxygen–hydrogen (Fig. 3) and hydrogen–hydrogen radial distribution functions (Fig. 4) for TIP4P-FQ and TIP4P models are also shown. The radial distribution functions for the SPC-FQ potential are shown in Figs. 5, 6, and 7. Again, the flexible charge $g_{OO}(r)$ shows more long-range correlation than the corresponding fixed charge model, but, in general, the SPC-FQ model does not give as accurate pair correlation functions as the TIP4P-FQ model. The number of nearest neighbors can be determined by integrating $g_{OO}(r)$ over the first peak. Experimentally, the first minimum occurs at 3.3 Å and using this value as the limit of the first peak gives essentially the same coordination number for all models—4.2 (SPC-FQ), 4.3 (TIP4P), and 4.4 (TIP4P-FQ, experiment, and SPC).

The average dipole moment $\langle\mu\rangle$ is increased for both fluctuating charge models over the corresponding fixed-charge models. The value of the liquid state dipole moment is not known experimentally. The experimental value for ice is 2.6 D.⁴² Theoretical studies which use potentials which have the correct dipole polarizability and quadrupole moments find a dipole moment of 2.5 (Ref. 18) and 2.45–2.7 D, depending on the details of the nonelectrostatic part of the potential (Ref. 43). Additionally, it has been observed that the dependence of the dielectric constant on the dipole moment is such that to have a dielectric constant close to 80, the potential must have a dipole moment in the range of 2.3 to 2.6 D.³⁷ The distributions of the dipole moment are shown in Fig. 8. The full width at half-maximum is 0.42 for SPC-FQ and 0.49 for TIP4P-FQ. The SPC geometry, with greater distances between the charge sites, is more polarizable and

therefore the distribution of the $|\mu|$ is broader. In the fluctuating charge models, the instantaneous dipole moment does not always lie along the C_2 direction (what we have previously defined as the z axis). The average of the component of the dipole moment along the C_2 axis μ_z for the TIP4P-FQ model is 2.59 D, which when compared to the total dipole moment of 2.62 D indicates that there are small fluctuations of the dipole moment away from the C_2 axis. For the SPC-FQ model, μ_z is 2.81 D and the total dipole moment is 2.83 D.

The static dielectric constant ϵ_0 for the FQ potentials, calculated from the fluctuations in the total dipole of the central simulation box \mathbf{M} according to³³

$$\epsilon_0 = \epsilon_\infty + \left(\frac{4\pi\rho}{3kT} \right) \left(\frac{\langle M^2 \rangle - \langle M \rangle^2}{N_{\text{molec}}} \right), \quad (4.3)$$

is 79 ± 8 for TIP4P-FQ and 116 ± 18 for SPC-FQ. Equation (4.3) was evaluated from a 1 ns run. The dielectric constant of the TIP4P-FQ model is in good agreement with experiment, which is consistent with earlier findings that models with a dipole moment of 2.6 D have a dielectric constant near 80.^{36,37,43} The SPC-FQ model is in poorer agreement due to the fact that the liquid state dipole moment is large. A large dipole moment^{21,24,25} and dielectric constant⁴⁴ are also seen in dipole polarizable SPC models. From this perspective, the TIP4P geometry is better than SPC.

The fluctuating charge models have a dielectric response characterized by an infinite frequency dielectric constant ϵ_∞ . Neumann and Steinhauser have derived expressions for cal-

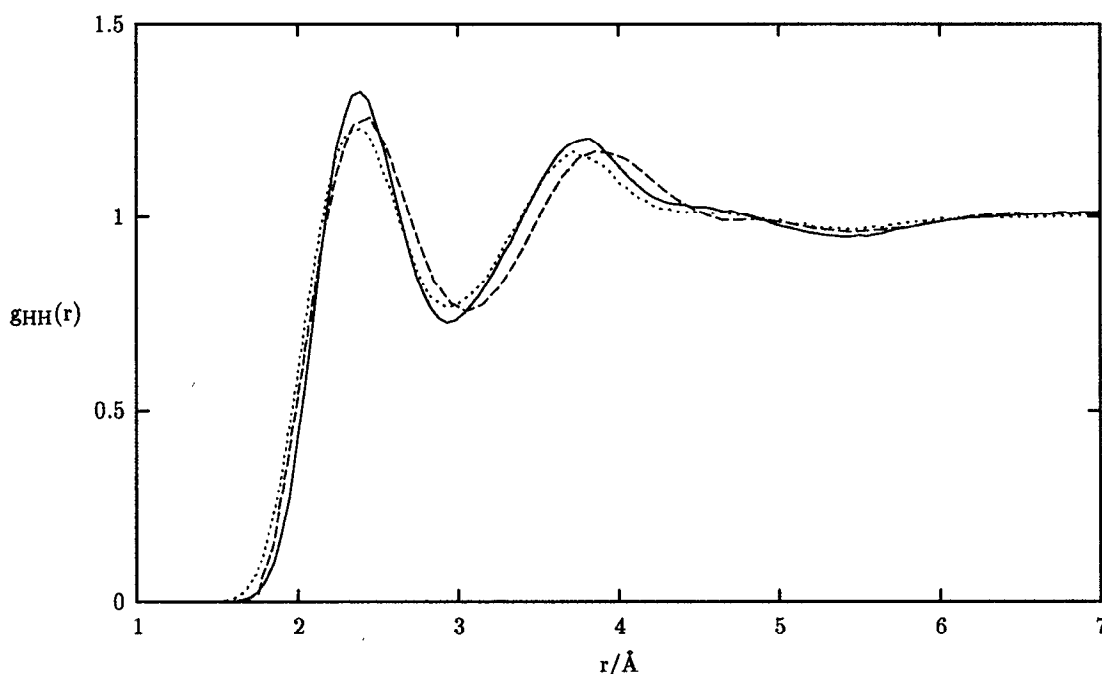


FIG. 4. Hydrogen–hydrogen radial distribution function for the TIP4P-FQ (solid line) and TIP4P (dotted line) potentials, compared to the neutron diffraction results of Soper and Phillips (dashed line).

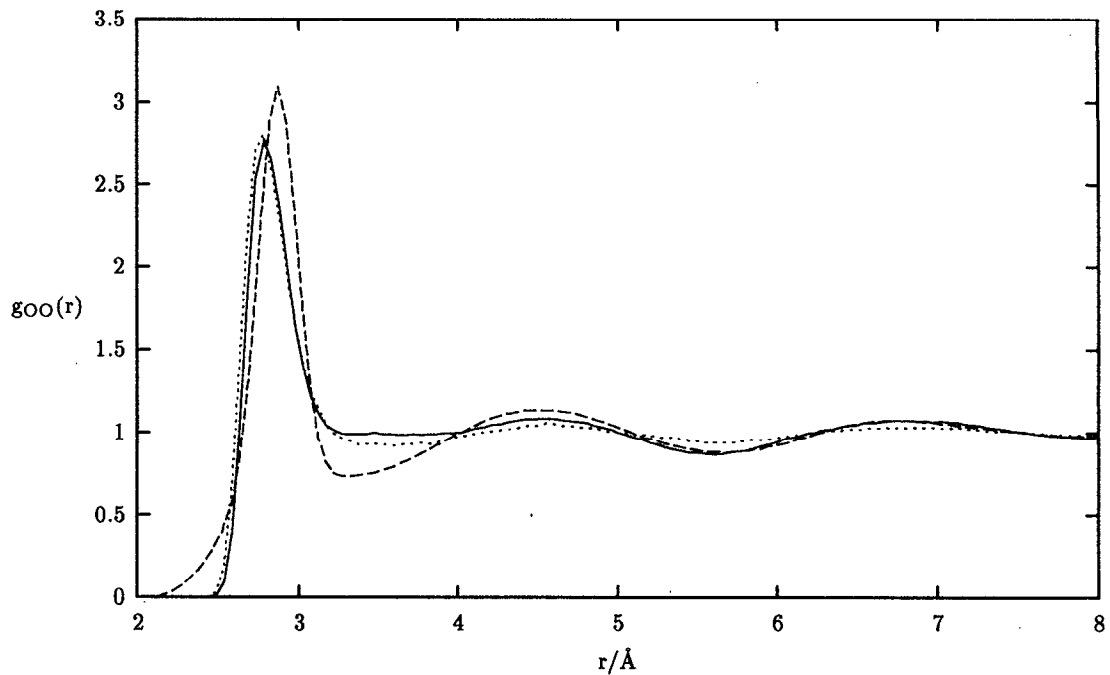


FIG. 5. Oxygen-oxygen radial distribution function for the SPC-FQ (solid line) and SPC (dotted line) potentials, compared to the neutron diffraction results of Soper and Phillips (dashed line).

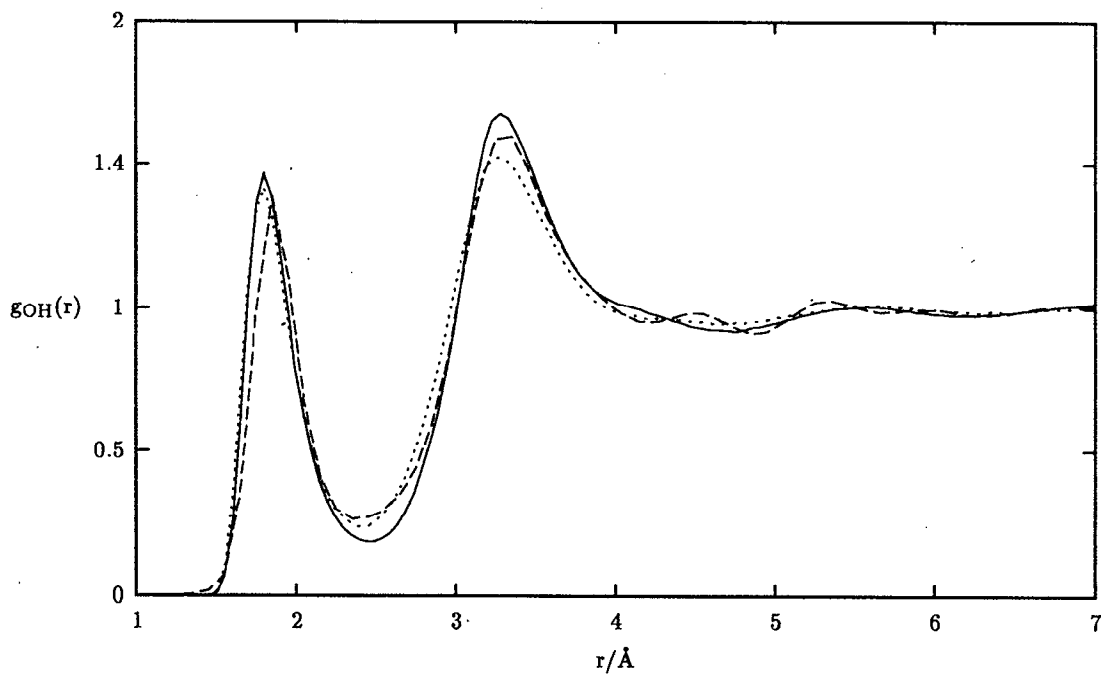


FIG. 6. Oxygen-hydrogen radial distribution function for the SPC-FQ (solid line) and SPC (dotted line) potentials, compared to the neutron diffraction results of Soper and Phillips (dashed line).

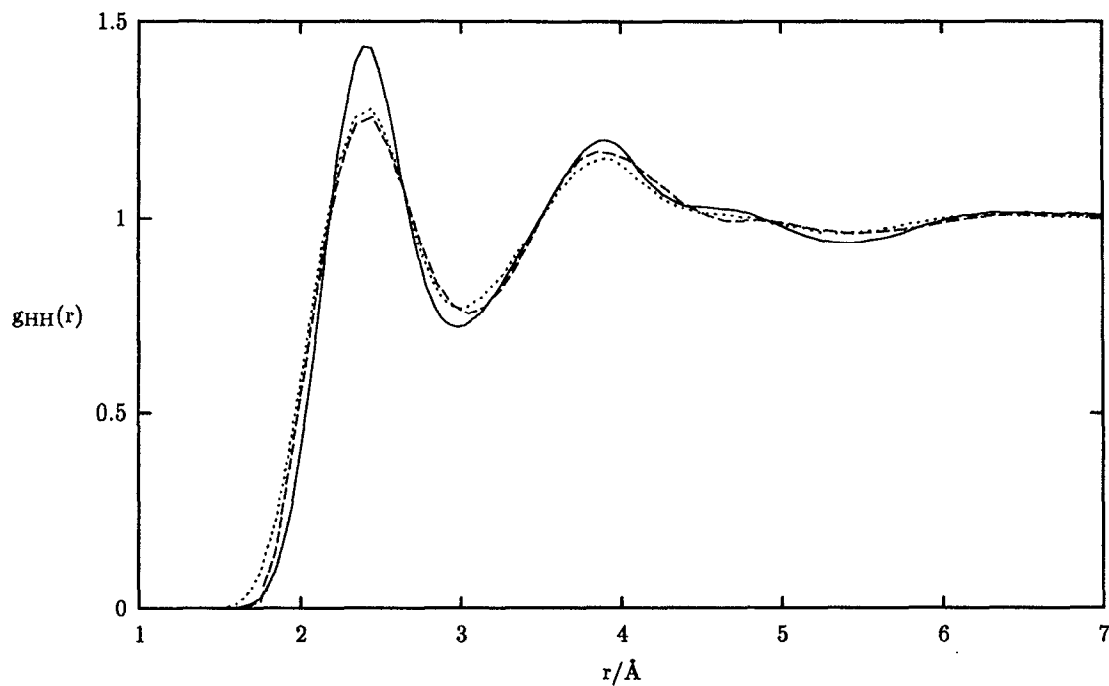


FIG. 7. Hydrogen-hydrogen radial distribution function for the SPC-FQ (solid line) and SPC (dotted line) potentials, comparing to the neutron diffraction results of Soper and Phillips (dashed line).

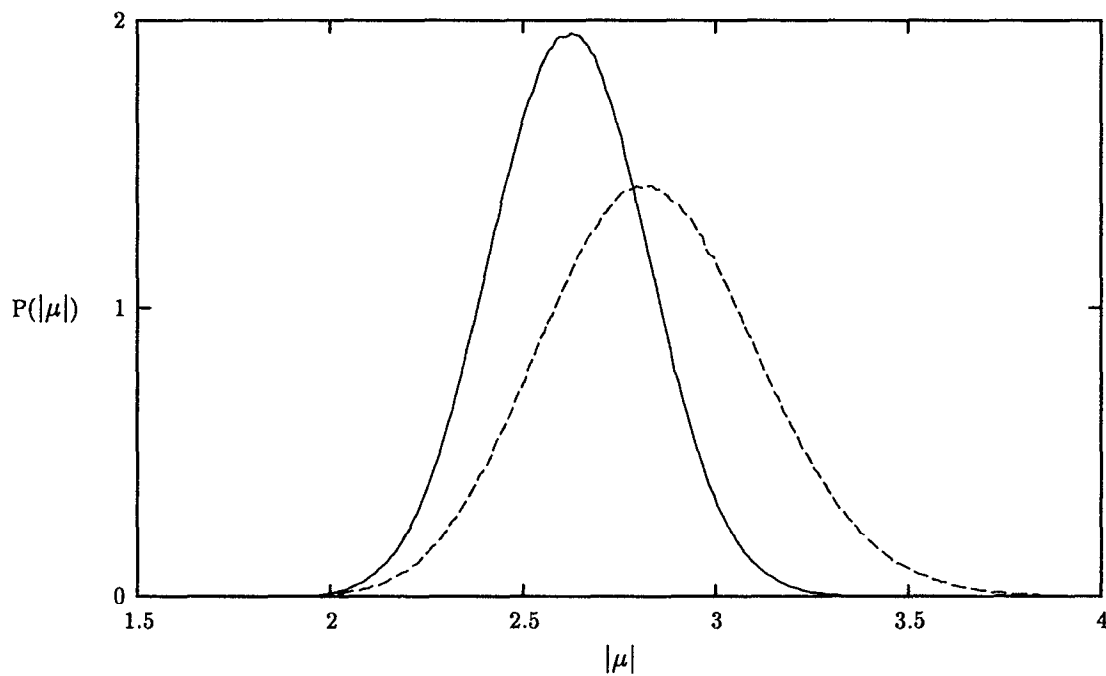


FIG. 8. Distribution of the absolute value of the dipole moments of the TIP4P-FQ (solid line) and SPC-FQ (dashed line) liquids.

culating ϵ_∞ for dipole polarizable models.⁴⁵ Expressions for ϵ_∞ for fluctuating charge models are similar. The Coulomb energy can be written as

$$U(\mathbf{Q}) = (\tilde{\chi}_H^0 - \tilde{\chi}_O^0) \mathbf{Q} \cdot \mathbf{I} + \frac{1}{2} \mathbf{Q} \cdot \mathbf{J} \cdot \mathbf{Q}, \quad (4.4)$$

$$J_{i\alpha,j\beta} = \begin{cases} 1/r_{i\alpha,j\beta} - 1/r_{i\alpha,jM} - 1/r_{iM,j\beta} + 1/r_{iM,jM}, & i \neq j \\ J_{\alpha\beta}(r_{i\alpha,j\beta}) - J_{\alpha O}(r_{i\alpha,jM}) - J_{O\beta}(r_{iM,j\beta}) + J_{OO}(r_{iM,jM}), & i = j \end{cases} \quad (4.5)$$

With the Ewald sum—which we are using in the present calculations—for the long range Coulomb interaction, each $1/r$ and $J_{\alpha\beta}$ interaction in Eq. (4.5) is replaced as follows:³³

$$1/r_{i\alpha,j\beta} \Rightarrow \text{erfc}(\kappa r_{i\alpha,j\beta})/r_{i\alpha,j\beta}$$

$$+ \frac{4\pi}{L^3} \sum_{\mathbf{G} \neq 0} \frac{1}{G^2} e^{-G^2/4\kappa^2} \cos(\mathbf{G} \cdot \mathbf{r}_{i\alpha,j\beta}),$$

$$J_{\alpha,\beta}(r_{i\alpha,i\beta}) \Rightarrow J_{\alpha,\beta}(r_{i\alpha,i\beta}) - \text{erf}(\kappa r_{i\alpha,i\beta})/r_{i\alpha,i\beta}$$

$$+ \frac{4\pi}{L^3} \sum_{\mathbf{G} \neq 0} \frac{1}{G^2} e^{-G^2/4\kappa^2} \cos(\mathbf{G} \cdot \mathbf{r}_{i\alpha,i\beta}).$$

The minimum energy charges are given by

$$\mathbf{Q} = -(\tilde{\chi}_H^0 - \tilde{\chi}_O^0) \mathbf{J}^{-1} \cdot \mathbf{I}, \quad (4.6)$$

where \mathbf{J}^{-1} is the inverse of \mathbf{J} . In the presence of a spatially homogeneous external electric field \mathbf{E} , the charges are

$$\mathbf{Q} = \mathbf{Q}^0 + \mathbf{J}^{-1} \cdot \delta \mathbf{r} \cdot \mathbf{E}, \quad (4.7)$$

where \mathbf{Q} is a $2N_{\text{molec}}$ dimensional vector containing the hydrogen charges (the oxygen charges are eliminated from the equation using the charge neutrality constraint), \mathbf{I} is the identity vector, and \mathbf{J} is a $(2N_{\text{molec}} \times 2N_{\text{molec}})$ matrix. The elements of \mathbf{J} are given by

where \mathbf{Q}^0 are the charges in the absence of the field and $\delta \mathbf{r}_{i\alpha} = \mathbf{r}_{i\alpha} - \mathbf{r}_{iO}$. The energy is

$$U = U^0 - \mathbf{M} \cdot \mathbf{E} - \frac{1}{2} \mathbf{E} \cdot \mathbf{A} \cdot \mathbf{E}, \quad (4.8)$$

where U^0 is the energy in the absence of the field and \mathbf{A} is the polarizability of the system given by

$$A_{i\alpha,j\beta} = \delta \mathbf{r}_{i\alpha} \cdot \delta \mathbf{r}_{j\beta} J_{i\alpha,j\beta}^{-1}. \quad (4.9)$$

Following Ref. 45, ϵ_∞ is

$$\epsilon_\infty = 1 + \frac{4\pi}{3V} \sum_{i=1}^{N_{\text{molec}}} \sum_{j=1}^{N_{\text{molec}}} \sum_{\alpha=2}^3 \sum_{\beta=2}^3 \langle A_{i\alpha,j\beta} \rangle. \quad (4.10)$$

Equation (4.10) was evaluated every 50 ps in the course of the simulations, which is a frequent enough sampling rate to provide a precise estimate of $\langle A_{i\alpha,j\beta} \rangle$. The value obtained for

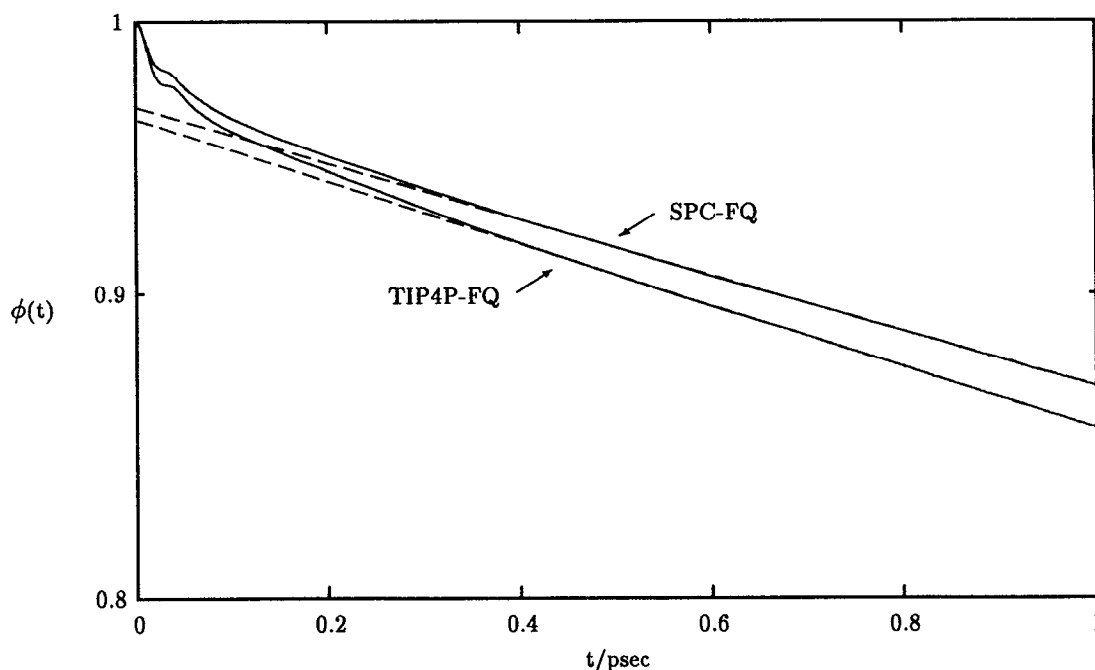


FIG. 9. Time autocorrelation function for the system dipole for the SPC-FQ (top line) and TIP4P-FQ (bottom line) models and the exponential long-time approximation (dash lines), shown on semilog axes.

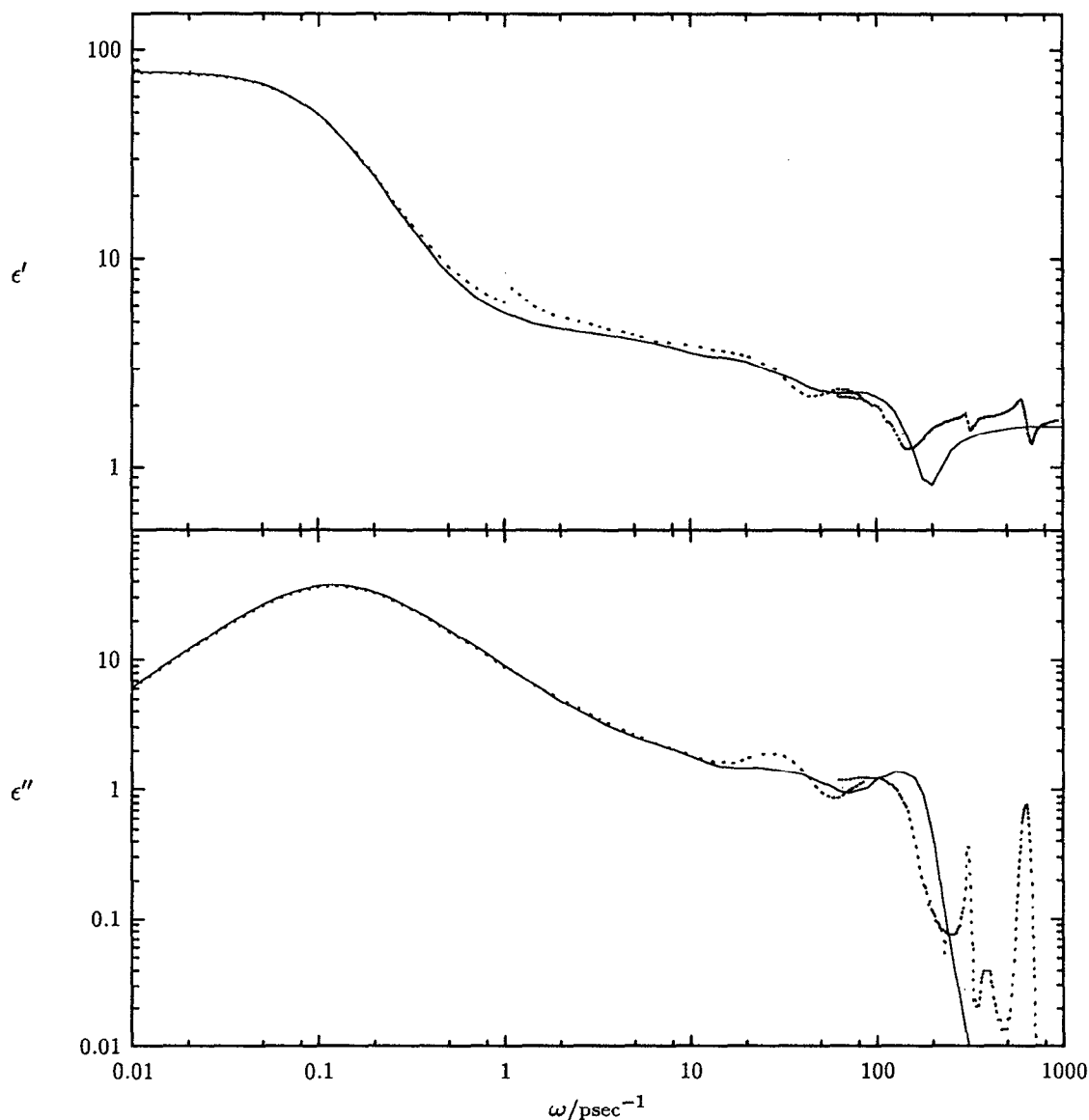


FIG. 10. Real (top) and imaginary (bottom) parts of the frequency dependent dielectric constant for the TIP4P-FQ model (solid lines), compared to experiment (dotted lines).

ϵ_∞ from both fluctuating charge models is about 1.6, close to the experimental value of 1.79.⁴⁶ ϵ_∞ is underestimated because the perpendicular polarizability α_{xx} is zero. To leading order in α , and thus $\epsilon_\infty - 1$, the total system polarizability \mathbf{A} is proportional to $\text{Tr}(\alpha)$.⁴⁵ It then follows that to order α ,

$$\frac{\epsilon_\infty(\text{FQ}) - 1}{\epsilon_\infty(\text{exact}) - 1} \approx \frac{\text{Tr}[\alpha(\text{FQ})]}{\text{Tr}[\alpha(\text{exact})]}, \quad (4.11)$$

which holds for the data from Tables II and III. Therefore, $\alpha_{xx} = 0$ produces an ϵ_∞ smaller than the experimental value.

The frequency dependent dielectric constant can be calculated from⁴⁵

$$\frac{\epsilon(\omega) - \epsilon_\infty}{\epsilon_0 - \epsilon_\infty} = 1 - i\omega \mathcal{L}_{i\omega}[\phi(t)] \quad (4.12)$$

where $\mathcal{L}_{i\omega}$ denotes the Laplace operator and $\phi(t)$ is the normalized time autocorrelation function of the system's total dipole ($\mathbf{M} = \sum \boldsymbol{\mu}_i$),

$$\phi(t) = \langle \mathbf{M}(t) \cdot \mathbf{M}(0) \rangle / \langle \mathbf{M}^2 \rangle. \quad (4.13)$$

$\phi(t)$ has a short-time oscillatory part, due to librational motions of the hydrogen atoms. At long times, $\phi(t)$ decays exponentially and the decay constant is the Debye relaxation time τ_D (see Fig. 9). In order to perform the Laplace transform to get $\epsilon(\omega)$, we set $\phi(t) = A \exp(-t/\tau_D)$ for times longer than 0.5 ps. The parameters A and τ_D were chosen to give a smooth interpolation between the calculated $\phi(t)$ and the exponential fit (see Fig. 9). The frequency dependent dielectric constant for the TIP4P-FQ model is shown in Fig. 10. The agreement with the experimental results⁴⁷⁻⁴⁹ is very

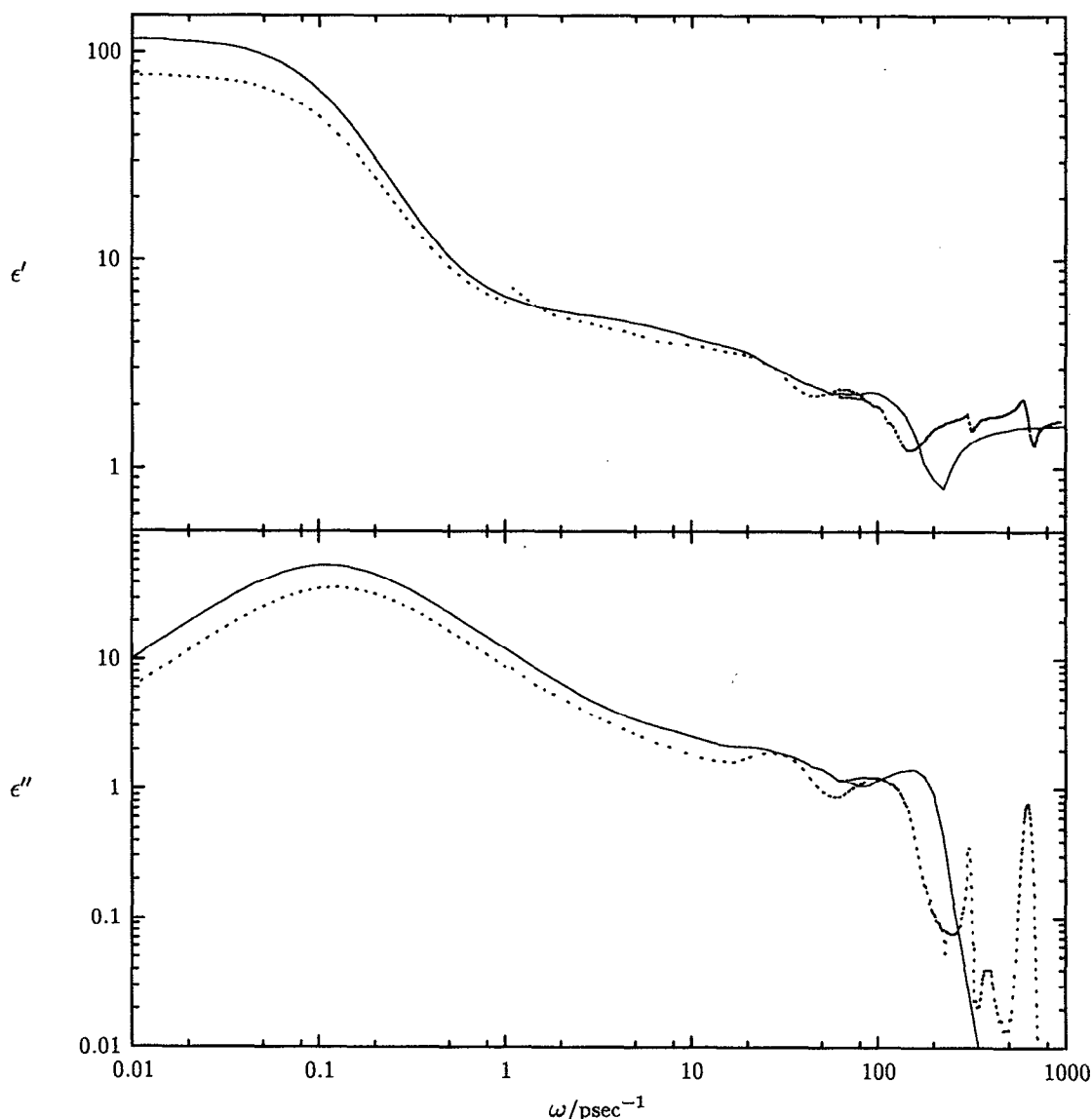


FIG. 11. Real (top) and imaginary (bottom) parts of the frequency dependent dielectric constant for the SPC-FQ model (solid lines), compared to experiment (dotted lines).

good. The close agreement in the low-frequency microwave range is due to the fact that the model gives accurate values of ϵ_0 and τ_D . The features at frequencies higher than 300 ps^{-1} are due to bond stretches and bends and so are not present in the rigid geometry models used here. The highest frequency feature given by the TIP4P-FQ model is the librational mode, which shows a peak in ϵ'' at 130 ps^{-1} . The experimental peak is at 90 ps^{-1} .⁴⁹ Another notable feature is at 25 ps^{-1} , which has been interpreted as a translational vibration of a water molecule in its cage of nearest neighbors.⁵⁰ This feature is not present in the spectrum for nonpolarizable water models such as TIP4P⁵¹ or Matsuoko-Clementi-Yoshimine.⁵² As argued by Neumann, this translational motion will not change the system's dipole moment much for nonpolarizable models, but for polarizable models, the translation motion will induce a change in the dipole moment.⁵¹ Therefore this feature can only be seen in

polarizable models. The fluctuating charge models support that argument. The frequency dependent dielectric constant for SPC-FQ is shown in Fig. 11. The agreement with experiment is not as good as the TIP4P-FQ model, primarily because the static dielectric constant is overestimated. The librational peak is at 160 ps^{-1} for the SPC-FQ model.

Lastly, we examine the dynamical properties of the fixed and fluc- q model potentials. In general, the flexible charge models have slower translational and rotational time scales than the fixed-charge models, due primarily to the stronger electrostatic interactions from the higher charges. The translational diffusion constant D is determined from the Einstein relation

$$D = \lim_{t \rightarrow \infty} \frac{1}{6t} \langle |\mathbf{r}_i^{\text{c.m.}}(t) - \mathbf{r}_i^{\text{c.m.}}(0)|^2 \rangle, \quad (4.14)$$

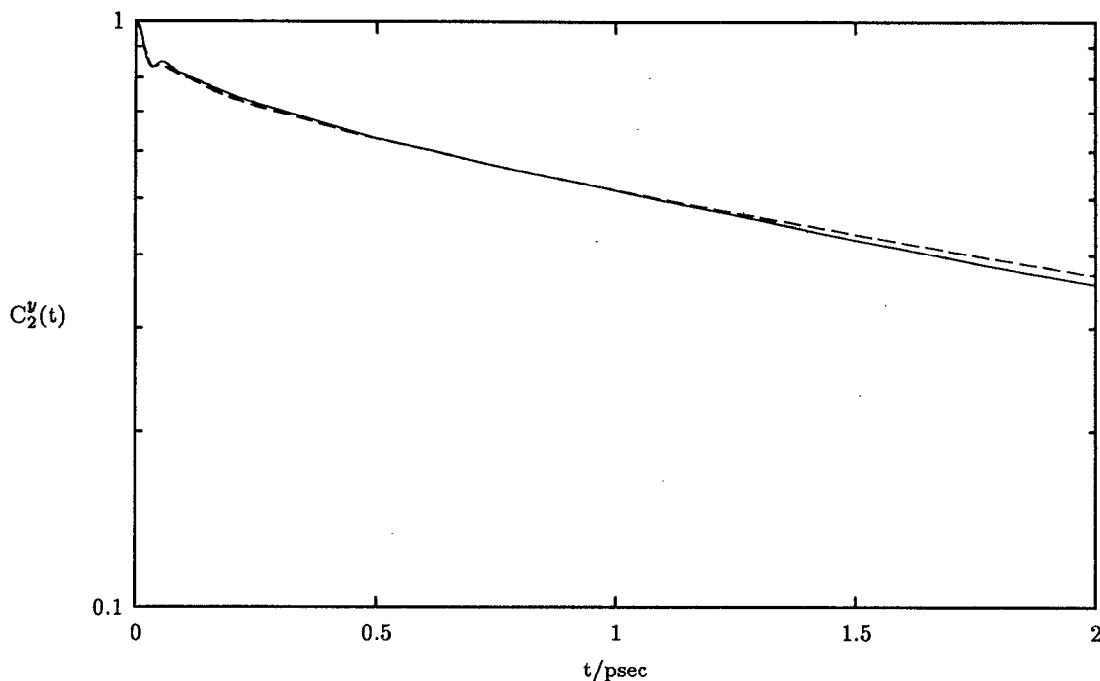


FIG. 12. Rotational correlation function for TIP4P-FQ (solid line) and SPC-FQ (dotted line).

where $\mathbf{r}_i^{\text{c.m.}}(t)$ is the position of the center of mass of molecule i at time t . The diffusion constants for the flexible-charge models are smaller than the fixed-charge models and closer to the experimental value (see Tables II and III). Rotational time constants are calculated from

$$C_l^\alpha(t) = \langle P_l[\mathbf{e}_i^\alpha(t) \cdot \mathbf{e}_i^\alpha(0)] \rangle, \quad (4.15)$$

where P_l is a Legendre polynomial and \mathbf{e}_i^α is a unit vector along molecule i 's principle axis of rotation.⁵³ Rotations around the axis connecting the hydrogen atoms (the y axis) can be measured by proton nuclear magnetic resonance (NMR). The zero frequency component of the Fourier transform of $C_2^y(t)$ gives the NMR relaxation time τ_{NMR} . The correlation function $C_2^y(t)$ has a long-range exponential decay, given by $A_2^y \exp(-t/\tau_2^y)$, and a short-range, oscillatory part (see Fig. 12). The zero frequency part of the Fourier transform of $C_2^y(t)$ is, to a good approximation, given by $A_2^y \tau_2^y$, since the short-range part will not contribute much to the transform. The flexible-charge models exhibit slower re-orientational dynamics than the fixed-charge models and are in closer agreement with the experimental value.⁵⁴

V. CONCLUSIONS

The fluctuating charge (fluc- q) water models, using either a TIP4P or SPC geometry, were shown to give important improvements over fixed-charge models. The electronic properties of the fluc- q models are such that in the gas phase they give the correct dipole moment (this is by construction), and in the liquid phase, the dielectric properties are well reproduced for a range of frequencies (see Figs. 10 and 11). The dielectric properties are best for the TIP4P-FQ model, which gives a static dielectric constant ϵ_0 , an infinite fre-

quency dielectric constant ϵ_∞ , and a Debye relaxation time τ_D close to the experimental values. The SPC-FQ model overestimates ϵ_0 , but ϵ_∞ and τ_D are accurate. The fluc- q models also show (at 25 ps^{-1}) a feature in the dielectric spectrum originating from translational motion of a water molecule in the cage of its neighbors. This is a feature not present in fixed-charge models.^{51,52} Translations will have a large effect on the system's dipole moment only for polarizable models, so this feature of $\epsilon(\omega)$ is an indication of the coupling between the electronic and nuclear degrees of freedom.

In addition, the fluc- q models give good estimates for the liquid-state radial distribution functions (see Figs. 2–7) and dynamical properties such as the diffusion constant and τ_{NMR} (see Tables II and III). Since the charges are not fixed to values which represent mean field values for a particular single-component phase, this method should be transferable to studies of heterogeneous systems in which deviations from the mean field charge values should be greater than in pure systems.¹⁸ The fluc- q method assigns two parameters to each element corresponding to the two terms in the energy expansion [Eq. (2.1)]. The first order term is the Mullikan electronegativity $\bar{\chi}$ and the second order term is determined by a Slater exponent ζ through the Coulomb overlap integral [Eq. (2.11)]. Extensions to more complex molecules would require additional terms for other elements, perhaps to be taken from other electronegativity equalization schemes.^{3–7}

All in all, the fluc- q water models are as successful as the best of the dipole polarizable models, such as SRWK-P,³⁷ the reduced effective representation,²³ and the polarizable SPC model of Dang.²⁴ The dipole polarizable models introduce an interaction (the dipole–dipole interaction) not

present in fixed-charge models, which, together with solving for the induced dipole moments, increases the CPU time by about a factor of 2 over fixed-charge models.^{23,26} The fluc- q method introduces no new interactions and the propagation of the charges using extended Lagrangian methods increases the computational cost by only a modest amount (about 1.1). The dynamical fluctuating charge method is therefore a tractable means for the inclusion of charge polarization effects and will be useful for the study of large systems, such as proteins in aqueous environments.

ACKNOWLEDGMENTS

This work was funded by a grant from the National Institutes of Health (GM 43340) and was done on the Thinking Machines CM-5 in the NIH Biotechnology Resource Center at Columbia University. S.J.S. was supported by a National Defense Science and Engineering Graduate Fellowship (DAAL 03-91-G-0277).

- ¹H. J. C. Berendsen, J. R. Grigera, and T. P. Straatsma, *J. Phys. Chem.* **91**, 6269 (1987).
- ²R. G. Parr and W. Yang, *Density-Functional Theory of Atoms and Molecules* (Oxford University, Oxford, 1989).
- ³L. Došen-Mičović, D. Jeremić, and N. L. Allinger, *J. Am. Chem. Soc.* **105**, 1716 (1983).
- ⁴W. J. Mortier, K. Van Genechten, and J. Gasteiger, *J. Am. Chem. Soc.* **107**, 829 (1985).
- ⁵K. T. No, J. A. Grant, and H. A. Scheraga, *J. Phys. Chem.* **94**, 4732 (1990).
- ⁶A. K. Rappé and W. A. Goddard, *J. Phys. Chem.* **95**, 3358 (1991).
- ⁷C. A. Reynolds, J. W. Essex, and W. G. Richards, *J. Am. Chem. Soc.* **114**, 9075 (1993).
- ⁸H. C. Andersen, *J. Chem. Phys.* **72**, 2384 (1980).
- ⁹M. Parrinello and A. Rahman, *Phys. Rev. Lett.* **45**, 1196 (1980).
- ¹⁰R. Car and M. Parrinello, *Phys. Rev. Lett.* **55**, 2471 (1985).
- ¹¹S. Nosé, *Mol. Phys.* **52**, 255 (1984).
- ¹²H. J. C. Berendsen, J. P. M. Postma, W. F. von Gunsteren, and J. Hermans, in *Intermolecular Forces*, edited by B. Pullman (Reidel, Dordrecht, 1981), p. 331.
- ¹³W. L. Jorgensen, J. Chandrasekhar, J. D. Madura, R. W. Impey, and M. L. Klein, *J. Chem. Phys.* **79**, 926 (1983).
- ¹⁴B. Jönsson, O. Edholm, and O. Teleman, *J. Chem. Phys.* **85**, 2259 (1986).
- ¹⁵K. Watanabe, M. Ferrario, and M. L. Klein, *J. Phys. Chem.* **92**, 819 (1988).
- ¹⁶K. A. Dill, D. E. Koppel, R. S. Cantor, J. D. Dill, D. Bendedouch, and S.-H. Chen, *Nature* **309**, 42 (1984).
- ¹⁷F. H. Stillinger and C. W. David, *J. Chem. Phys.* **69**, 1473 (1978).
- ¹⁸P. Barnes, J. L. Finney, J. D. Nicholas, and J. E. Quinn, *Nature* **282**, 459 (1979).
- ¹⁹J. A. C. Rullman and P. T. van Duijnen, *Mol. Phys.* **63**, 451 (1988).
- ²⁰M. Sprik and M. L. Klein, *J. Chem. Phys.* **89**, 7556 (1988).
- ²¹P. Ahlström, A. Wallqvist, S. Engström, and B. Jönsson, *Mol. Phys.* **68**, 563 (1989).
- ²²P. Cieplak, P. Kollman, and T. Lybrand, *J. Chem. Phys.* **92**, 6755 (1990).
- ²³A. Wallqvist and B. J. Berne, *J. Phys. Chem.* **97**, 13 841 (1993).
- ²⁴L. X. Dang, *J. Chem. Phys.* **97**, 2659 (1992).
- ²⁵D. N. Bernardo, Y. Ding, K. Krogh-Jespersen, and R. M. Levy, *J. Chem. Phys.* (in press).
- ²⁶D. van Belle, M. F. G. Lippens, and S. J. Wodak, *Mol. Phys.* **77**, 239 (1992).
- ²⁷R. T. Sanderson, *Science* **114**, 670 (1951).
- ²⁸M. Sprik, *J. Phys. Chem.* **95**, 2283 (1991).
- ²⁹P. E. Blochl and M. Parrinello, *Phys. Rev. B* **45**, 9413 (1992).
- ³⁰E. S. Fois, J. I. Penman, and P. A. Madden, *J. Chem. Phys.* **98**, 6361 (1993).
- ³¹M. Tuckerman, B. J. Berne, and G. J. Martyna, *J. Chem. Phys.* **97**, 1990 (1992).
- ³²In all formulas involving the Coulomb energy (e.g., $Q_{i\alpha}Q_{j\beta}/r_{i\alpha,j\beta}$ or $Q_{i\alpha}Q_{j\beta} J_{\alpha,\beta}$), a factor of $1/4\pi\epsilon_0$ is assumed, where ϵ_0 is the vacuum permittivity.
- ³³M. P. Allen and D. J. Tildesley, *Computer Simulation of Liquids* (Oxford University, Oxford, 1987).
- ³⁴D. L. Lynch, S. W. Rick, M. A. Gomez, B. W. Spath, J. D. Doll, and L. R. Pratt, *J. Chem. Phys.* **97**, 5177 (1992).
- ³⁵These results are based on a test version of the software where the emphasis was on providing functionality and the tools necessary to begin testing the CM-5 with vector units. This software release has not had the benefit of optimization or performance tuning and, consequently, is not necessarily representative of the performance of full version of this software.
- ³⁶K. Watanabe and M. L. Klein, *Chem. Phys.* **131**, 157 (1989).
- ³⁷M. Sprik, *J. Chem. Phys.* **95**, 6762 (1991).
- ³⁸W. F. Murphy, *J. Phys. Chem.* **67**, 5877 (1977).
- ³⁹U. Dinar, *J. Phys. Chem.* **97**, 7894 (1993).
- ⁴⁰A. K. Soper and M. G. Phillips, *Chem. Phys.* **107**, 47 (1986).
- ⁴¹A. K. Soper and J. Turner, *Int. J. Mod. Phys. B* **7**, 3049 (1993).
- ⁴²C. A. Coulson and D. Eisenberg, *Proc. R. Soc. London Ser. A* **291**, 445 (1966).
- ⁴³S. L. Carnie and G. N. Patey, *Mol. Phys.* **47**, 1129 (1982).
- ⁴⁴D. E. Smith and L. X. Dang, *J. Chem. Phys.* **100**, 3757 (1994).
- ⁴⁵M. Neumann and O. Steinhauser, *Chem. Phys. Lett.* **106**, 563 (1984).
- ⁴⁶A. D. Buckingham, *Proc. R. Soc. London Ser. A* **238**, 235 (1956).
- ⁴⁷U. Kaatzte and V. Uhlendorf, *Z. Phys. Chem. N.F.* **126**, 151 (1981).
- ⁴⁸M. N. Afsar and J. B. Hasted, *J. Opt. Soc. Am.* **67**, 902 (1977).
- ⁴⁹A. N. Rusk, D. Williams, and M. R. Querry, *J. Opt. Soc. Am.* **61**, 895 (1971).
- ⁵⁰G. E. Walrafen, in *Water—A Comprehensive Treatise*, edited by F. Franks (Plenum, New York, 1972), Vol. 1.
- ⁵¹M. Neumann, *J. Chem. Phys.* **85**, 1567 (1986).
- ⁵²M. Neumann, *J. Chem. Phys.* **82**, 5663 (1985).
- ⁵³R. W. Impey, P. A. Madden, and I. R. McDonald, *Mol. Phys.* **46**, 513 (1982).
- ⁵⁴J. Jonas, T. DeFries, and D. J. Wilber, *J. Chem. Phys.* **65**, 582 (1976).
- ⁵⁵A. C. Shepard, Y. Beers, G. P. Klein, and L. S. Rothman, *J. Chem. Phys.* **59**, 2254 (1973).
- ⁵⁶J. A. Odutola and T. R. Dyke, *J. Chem. Phys.* **72**, 5062 (1980).
- ⁵⁷K. Krynicki, C. D. Green, and D. W. Sawyer, *Discuss. Faraday Soc.* **66**, 199 (1978).
- ⁵⁸H. E. Alper and R. M. Levy, *J. Chem. Phys.* **91**, 1242 (1989).